Open access • Proceedings Article • DOI:10.2514/6.2000-4011

Hyper-X Research Vehicle (HXRV) Experimental Aerodynamics Test Program Overview — Source link

Scott D. Holland, William C. Woods, Walter C. Engelund

Institutions: Langley Research Center

Published on: 01 Jan 2000

Topics: Aerodynamics, Scramjet, Propulsion and Hypersonic speed

AIAA 2000-4011
Hyper-X Research Vehicle (HXRV) Experimental Aerodynamics Test Program Overview

Scott D. Holland,
William C. Woods,
Walter C. Engelund

NASA Langley Research Center
Hampton, VA

AIAA 18th Applied Aeronautics Conference
August 14-17, 2000
Denver, Colorado

HYPER-X RESEARCH VEHICLE (HXRV) EXPERIMENTAL AERODYNAMICS TEST PROGRAM OVERVIEW

Scott D. Holland*, William C. Woods**, and Walter C. Engelund***
NASA Langley Research Center, Hampton, VA

Abstract

This paper provides an overview of the experimental aerodynamics test program to ensure mission success for the autonomous flight of the Hyper-X Research Vehicle (HXRV). The HXRV is a 12-ft long, 2700 lb lifting body technology demonstrator designed to flight demonstrate for the first time a fully airframe integrated scramjet propulsion system. Three flights are currently planned, two at Mach 7 and one at Mach 10, beginning in the fall of 2000. The research vehicles will be boosted to the prescribed scramjet engine test point where they will separate from the booster, stabilize, and initiate engine test. Following 5+ seconds of powered flight and 15 seconds of cowl-open tares, the cowl will close and the vehicle will fly a controlled deceleration trajectory which includes numerous control doublets for in-flight aerodynamic parameter identification. This paper reviews the preflight testing activities, wind tunnel models, test rationale, risk reduction activities, and sample results from wind tunnel tests supporting the flight trajectory of the HXRV from hypersonic engine test point through subsonic flight termination.

Nomenclature

α angle-of-attack (degrees)
β sideslip angle (degrees)
b_{ref} Hyper-X vehicle reference span
C_D Drag force coefficient ($\frac{Drag}{q_\infty S_{ref}}$)
C_L Lift force coefficient ($\frac{Lift}{q_\infty S_{ref}}$)
$C_{L\alpha}$ Lift coefficient derivative with respect to angle of attack (per degree)
C_l Rolling moment coefficient ($\frac{rolling\ moment}{q_\infty S_{ref} b_{ref}}$)
$C_{l\delta a}$ Rolling moment coefficient derivative with respect to aileron deflection (per degree)
$C_{l\beta}$ Rolling moment coefficient derivative with respect to sideslip angle (per degree)
C_m Pitching moment coefficient ($\frac{pitching\ moment}{q_\infty S_{ref} l_{ref}}$)
$C_{m\alpha}$ Pitching moment coefficient derivative with respect to angle of attack (per degree)
C_n Yawing moment coefficient ($\frac{yawing\ moment}{q_\infty S_{ref} b_{ref}}$)
$C_{n\beta}$ Yawing moment coefficient derivative with respect to sideslip angle (per degree)
$C_{n\delta_a}$ Yawing moment coefficient derivative with respect to aileron deflection (per degree)
C_Y Side force coefficient ($\frac{side\ force}{q_\infty S_{ref}}$)
$C_{Y\beta}$ Side force coefficient derivative with respect to sideslip angle
$C_{Y\delta a}$ Side force coefficient derivative with respect to aileron deflection (per degree)
δ_{rw} right full-flying wing deflection, degrees
δ_{lw} left full-flying wing deflection, degrees
δ_a aileron deflection (differential horizontal tail: $\delta_{rw} - \delta_{lw}$), degrees
δ_e elevon deflection (symmetric horizontal tail: $(\delta_{rw} + \delta_{lw})/2$), degrees
δ_{rr} right rudder deflection, degrees
δ_{lr} left rudder deflection, degrees
δ_r rudder deflection $(\delta_{rr} + \delta_{lr})/2$, degrees
l_{ref} Hyper-X vehicle reference length
q_∞ freestream dynamic pressure ($1/2\,\rho_\infty V_\infty^2$)
S_{ref} Hyper-X vehicle reference area

---

*Assistant Branch Head, Aerothermodynamics Branch, Senior Member AIAA.
**Aerothermodynamics Branch, Associate Fellow, AIAA.
***Vehicle Analysis Branch, Senior Member, AIAA.

Introduction

The goal of the Hyper-X Program is to demonstrate and validate the technologies, the experimental techniques, and computational methods and tools for design and performance predictions of hypersonic aircraft with airframe-integrated hydrogen fueled, dual-mode combustion scramjet propulsion systems (Ref. 1). Accomplishing this goal requires flight demonstration of a hydrogen-fueled scramjet powered hypersonic aircraft. This first-of-its-kind effort is truly pioneering in that, although hypersonic propulsion systems have been studied in the laboratory environment for over 40 years, one has never before been flight tested on a complete airframe-integrated vehicle configuration. In order to meet budget and schedule, the flight test vehicle design leveraged existing databases and off-the-shelf subsystem components wherever possible (Ref. 2).

The design evolution of the Hyper-X configuration used, as a starting point, the extensive National Aerospace Plane (NASP) database and experience, as well as follow-on mission study programs (e.g., Ref. 3). In a sense, the Hyper-X design development was the reverse of the NASP development. The NASP program failed to produce a flight vehicle due in part to insufficient technology development. The Hyper-X design development looked forward to a 200-foot operational "vision vehicle" (developed in the study of Ref. 4) but sought to design, build, and fly a minimum size flight research vehicle (as size is a major cost driver – Ref. 2) to demonstrate the technologies and design methodologies necessary to develop an operational "global reach" endoatmospheric hypersonic cruise vehicle. Such a vision vehicle could contribute to key national civilian and military requirements of routine, cost-effective access to space, and endoatmospheric, rapid-response, global reach operations. Preliminary design studies performed by NASA in early FY95 indicated that a 12 foot vehicle could be "smart scaled" from the 200 foot operational concept and still demonstrate scramjet powered acceleration (Ref. 2). Conceptual design trade studies were performed by McDonnell Douglas Aerospace (MDA – now Boeing-St. Louis) under contract to NASA (Ref. 5) between February and May, 1995. MDA completed a preliminary design between March and October, 1996 under Phase III of the Dual-Fuel Airbreathing Hypersonic Vehicle Design Study contract (Ref. 6). This preliminary design, which included basic structural design, thermal protection system selection, identification of major system/subsystem components and potential vendors, preliminary packaging, power requirements, stage separation approach, booster integration, and flight test planning, became the government candidate vehicle for the Hyper-X program. In July 1996, the Hyper-X program was approved by NASA Headquarters Code R (Aeronautics), and a request for proposals (RFP), based on the government candidate vehicle, was released in October 1996. The Hyper-X Launch Vehicle (HXLV) booster development contract was awarded to Orbital Sciences Corporation in February 1997 and the Hyper-X Research Vehicle (HXRV) development contract was awarded to MicroCraft, Inc. in March 1997.

Prior to the release of the RFP, the experimental aerodynamics program focused on configuration screening and preliminary database development in support of control law development and preliminary trajectory evaluations (including some Monte Carlo analyses) for inclusion in the RFP. Following contract award, the experimental aerodynamics program focused on configuration optimization/ maturation and benchmarking for each phase of the flight trajectory. This paper will describe the nominal trajectory and will review the extensive wind tunnel test program supporting the aero database development (described in Ref. 7) along that trajectory.

Mission Profile

The nominal Hyper-X flight trajectories each begin with a boost to the scramjet engine test conditions on a modified version of an Orbital Sciences Corporation Pegasus Hybrid rocket. The HXRV is attached to the first stage of the Pegasus rocket by means of a conically shaped adapter. This mated configuration (the HXRV, the adapter, and the booster) is referred to as the Hyper-X Launch Vehicle (HXLV) or "stack" configuration and is shown in Figure 1.

Figure 1. Hyper-X Launch Vehicle (HXLV) Configuration

The HXLV is carried aloft under the wing of NASA's B-52 where, in the case of the first two Mach 7

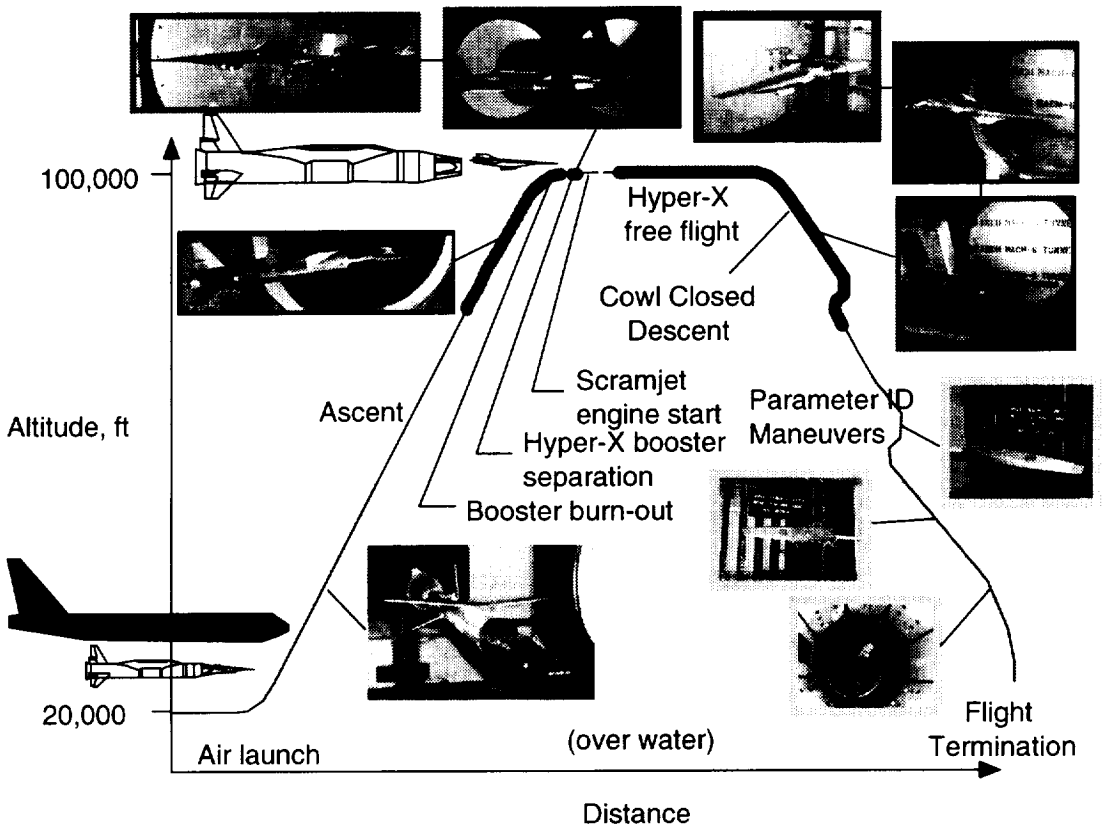

Figure 2. Nominal Mach 7 Hyper-X Flight Profile Superimposed with Wind Tunnel Test Photographs

experiments, it is dropped at an altitude of approximately 20,000 ft and a Mach number of 0.5. Shortly after drop, the booster solid rocket motor is ignited and the HXLV flies a nominal ascent profile to the HXRV test point as indicated in Figure 2. At a point just prior to the scramjet engine test, the Hyper-X flight vehicle is separated from the launch vehicle. The entire stage separation sequence, which occurs over a period of less than 500 milliseconds, presents several extreme technical challenges in addition to the basic ones associated with demonstrating the Hyper-X scramjet engine operation and performance. Details regarding the stage separation strategies and associated hardware simulation and testing can be found in Ref. 8. Details of the experimental test program for stage separation can be found in Ref. 9.

Immediately following the stage separation event, the HXRV control system will stabilize the vehicle and the scramjet test portion of the experiment will begin. The scramjet engine inlet door will be opened, and the scramjet fueling sequence will commence. A combination of silane (SiH_4) and gaseous hydrogen (H_2) is injected into the combustor region, resulting in powered scramjet engine operation. Silane is used only during the initial ignition process, after which pure hydrogen is injected and combusted. After the fuel is depleted, the flight vehicle will record several seconds of engine-off aerodynamic tare data, then the inlet cowl door will be shut and the vehicle will perform a series of aerodynamic parameter identification maneuvers at hypersonic and supersonic flight conditions. These maneuvers will allow the basic aerodynamic stability and control characteristics of the airframe to be estimated from the flight data, which will then be compared with the preflight predictions developed using the ground based wind tunnel testing and analytical and computational methods. The vehicle will then fly a controlled deceleration trajectory, dissipating energy by performing a series of S-turns, prior to flight termination at low subsonic conditions.

Model Design and Wind Tunnel Test Philosophy

Budget and schedule considerations placed significant constraints on the wind tunnel test activities. As the configuration matured, each latest revision had to be validated in the launch configuration, stage separation configuration, and research vehicle configuration across a range of Mach numbers. The testing program can be viewed as having three phases: screening, optimizing, and benchmarking. Early in the program when the configuration was evolving most rapidly, the program took advantage of rapid prototyping fabrication techniques to allow quick screening of several configurations, often in parallel, often for several phases of the flight, simultaneously. These early "quick look" models gained a schedule advantage (design and fabrication turn-around time) at a cost of limited parametrics and model fidelity. These models were designed to bracket the anticipated flight envelope to ensure that the vehicle was capable of trimmed, controlled flight at the desired test point. As the configuration matured, the program invested the additional time and resources to produce higher fidelity models with more parametrics to define the control effectiveness over a range of anticipated flight operation. The aero database was continually updated as data from higher fidelity models supplanted older data. To minimize total cost, the higher fidelity models were designed for maximal flexibility with minimal part count, sized for use in multiple facilities, and constructed to be cannibalized for use in follow-on models. These trades almost always resulted in a reduction in model scale, which created challenges in obtaining parametrics sufficient to address control effectiveness and control surface interactions. Simulation results based on the data from this intermediate set of models aided in the definition of parametric requirements for a specialized set of larger-scale models designed to benchmark the control effectiveness and interactions at levels fine enough to resolve nonlinearities in the aerodynamics across the entire range of anticipated flight (complete trajectory), including off-design conditions sufficiently broad to encompass the simulation dispersions. Testing resources for these models were allocated in accordance with a three-tier program prioritization (Ref. 10). The highest priority wind tunnel data are those that are required to get the vehicle to scramjet-powered test condition. This includes the following phases (and supporting wind tunnel test conditions): boost (Mach 0.8 to Mach 10); stage separation (Mach 6 and 10, which bracket the flight test conditions at Mach 7 and 10); and operation of the research vehicles at test conditions (Mach 6 and 10). Second priority was given to the research vehicle flight back to high subsonic speeds (Mach 4.6 to ~0.8). The lowest priority was subsonic operation of the research vehicle, since landing/ recovery was not required as part of this program.

Figure 2 shows the flight trajectory, with model photographs superimposed on the portions of the trajectory addressed. This figure will serve as a roadmap for the discussion of the experimental aerodynamics program as it relates to the HXRV. Since its inception in 1996, the extensive wind tunnel testing program to evolve and benchmark the current configuration across all phases of the flight trajectory has utilized 15 models in nine wind tunnels (both government and industry) with a total occupancy of more than 91 weeks. The configuration development is backed by more than 5800 wind tunnel runs. In order to assess the launch vehicle aerodynamic characteristics from B-52 dispense to stage separation, tests included several entries in the Lockheed-Martin Vought High Speed Wind Tunnel (Grand Prairie, TX) and several entries in NASA Langley's 16-Foot Transonic Tunnel, 20-Inch Mach 6 Air Tunnel, and 31-Inch Mach 10 Air Tunnel. (The repeated entries over the span of three years with multiple strain-gauge force and moment balances demonstrated overall measurement system stability which, along with the within-test repeatability and estimates for wind tunnel uncertainty, fed into the flight aerodynamics database uncertainty model.) The results from these tests and their incorporation into the launch vehicle aerodynamic database are discussed in Ref. 11. Preliminary analysis of the interference aerodynamics during the separation event was conducted using the HXRV and the adapter portion of the booster in the 20-Inch Mach 6 and 31-Inch Mach 10 Tunnels. These results led to extensive testing in the Arnold Engineering Development Center von Karman Gas Dynamics Facility (AEDC-VKF) Tunnel B at Mach 6. Six-component force and moment data were simultaneously obtained on the HXRV and booster+adapter combination in close proximity to each other. These tests made use of the AEDC captive trajectory system (CTS) rig. The details of these tests are presented in Ref. 9; a complementary CFD analysis of the stage separation is provided in Ref. 12. Due to the small size of the aerodynamic force and moment models, inlet-open testing (unpowered or powered using a simulant gas technique (Ref. 13)) was not possible. Cowl-open, fuel-on aerodynamic increments are addressed in a comprehensive CFD study (Ref. 14), which has been experimentally verified at several discrete flight test conditions by a full-scale propulsion flowpath test conducted in the NASA Langley 8-Foot High Temperature Tunnel (Ref. 15). Hypersonic cowl-closed flight stability and control (both immediately before and immediately after engine test) has been the

emphasis of several entries into the 20-Inch Mach 6 and 31-Inch Mach 10 Tunnels, along with a few runs piggybacked on the stage separation test at AEDC VKF Tunnel B. Early in the program, supersonic and transonic decent aerodynamics were evaluated in the McDonnell Douglas (now Boeing) – St. Louis Polysonic Wind Tunnel. As the configuration matured, these tests were superceded by tests using a larger, higher fidelity model with very fine gradations in surface control increments in the NASA Langley Unitary Plan Wind Tunnel Test Section 2 (4.6 < Mach < 2.5), Test Section 1 (2.1 < Mach < 1.6), and the 16-Foot Transonic Tunnel (1.2 < Mach < 0.6).

HXRV Decent Aerodynamics

It would be impossible to present in this brief overview paper the results from the entire Hyper-X experimental test program. This section will focus first on the aerodynamic tests performed to characterize the aerodynamics at Mach 6, in deference to the first flight, which will be at a Mach 7 engine test point. This will be followed by a summary of the across-the-speed-regime aerodynamic characteristics presented in the form of stability derivatives at selected points along the descent trajectory.

Mach 6 HXRV Aerodynamic Characteristics

The first attempts at defining the hypersonic aerodynamics of the Hyper-X Research Vehicle made use of an 8.33% (12-inch) keel line 3 (KL3) model shown in Figure 3. In keeping with the multi-use design philosophy, this model was sized to permit a clam-shell adapter to be affixed to the sting to provide an initial assessment of the order of magnitude of the stage separation interference effects. The model parametrics included symmetric and differential wing deflections (which serve as elevator and aileron control, respectively) and rudder deflections in coarse (10 deg) increments but bracketed the expected deflection requirements. When the configuration maturation concluded, a 12.5% (18-inch) high fidelity model (largest scale possible defined by wind tunnel blockage concerns) was designed with parametric capabilities including wing deflections in 2.5 deg increments from –20 to +20 deg and rudder deflections in 5 deg increments from –20 to +20 deg. Also in keeping with the multi-use design philosophy, this model was designed to address support interference as part of a risk reduction activity.

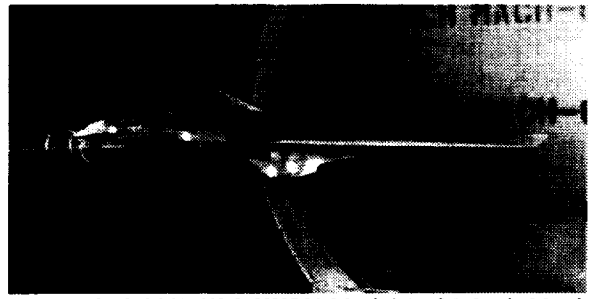

Figure 3. 8.33% KL3 HXRV Model in 20-Inch Mach 6 Tunnel

The basic longitudinal aerodynamic characteristics for the HXRV airframe (inlet door closed configuration) at Mach 6 conditions are shown in Fig. 4. The experimental results, obtained on the higher fidelity 12.5% scale (18-inch) model in the most recent test entry in the NASA LaRC 20-Inch Mach 6 Air Tunnel, indicate well-behaved, relatively linear lift characteristics over the anticipated flight angle-of-attack and elevator deflection angle range. Drag coefficient data are also shown to be well-behaved with angle-of-attack and elevator deflection angle. The pitching moment coefficient data, shown as a function of angle-of-attack for elevator deflection angles between 0 and 20 degrees, indicate an airframe with positive longitudinal stability (negative Cm_α slope) up to angles-of-attack of approximately eight degrees. At angles-of-attack beyond eight degrees the configuration becomes neutrally stable, based upon the moment reference location of 46% of vehicle length (which corresponds to the design c.g. of the flight vehicle). An elevator deflection angle of approximately seven degrees is required to trim the vehicle at the nominal flight angle-of-attack of two degrees for the inlet closed configuration.

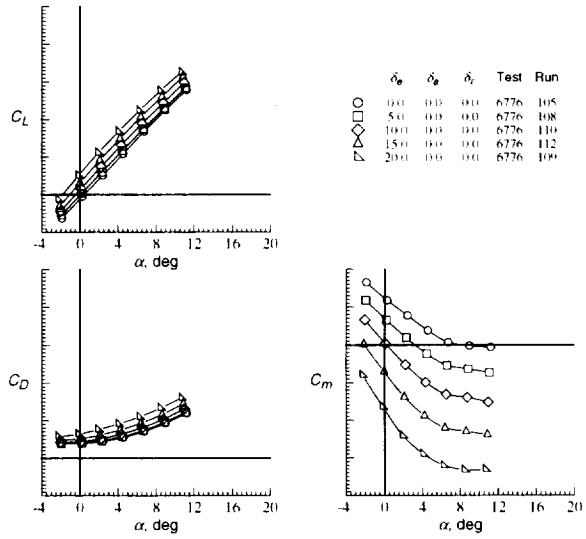

Figure 4. HXRV Mach 6 basic longitudinal aerodynamic characteristics (Wind Tunnel results)

The primary intent of the stage separation tests at AEDC was to develop the two body interference aerodynamic models required to support the stage separation simulation activities (see Refs. 8 and 9 for further discussion). As part of that test, data on the HXRV alone (and booster alone) were also obtained. The HXRV was supported by a blade mounted strut in the AEDC test, rather than by a conventional sting mount, in order that the flowfield interference effects in the region surrounding the nozzle and base of the HXRV and the HXLV adapter were properly modeled. In order to account for the effects of the blade mounted strut hardware used in the AEDC test, a separate test entry in the NASA Langley 20-Inch Mach 6 Tunnel was conducted at the same test conditions as at AEDC. As part of the Langley test, a sting mounted HXRV model was tested with a removable non-metric dummy blade, such that the force and moment increments associated with the AEDC blade mount could be computed. A photograph of the blade and sting mount parametric model is shown in Figure 5.

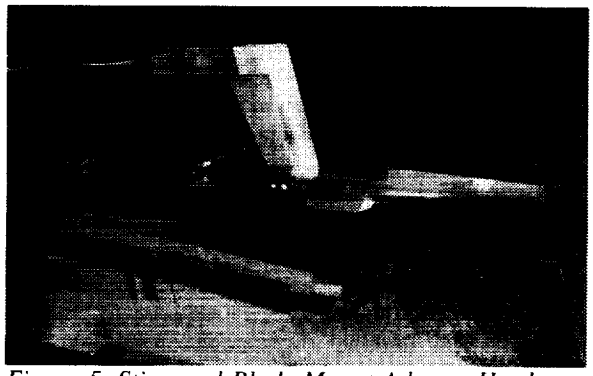

Figure 5. Sting and Blade Mount Adapter Hardware for the HXRV Wind Tunnel Tests

During this same test entry, the HXRV model was blade mounted and tested in the presence of a removable non-metric dummy sting, so that a corresponding sting mount increment could be computed. An example of the results of this series of tests are shown in Figure 6, in which the pitching moment data are shown for the HXRV configuration with the sting only, blade only, sting + dummy blade, and blade + dummy sting. The effect of the blade mount on pitching moment is rather dramatic. The primary influence of the presence of the blade is to pressurize the upper surface aft of the c.g., yielding a nose-up pitching moment increment. From this series of tests, a set of blade mount increments were derived by taking the difference of the sting mount + dummy blade results and the sting alone data. These increments were then applied to the AEDC stage separation test data to account for the blade interference effects on the forces and moments on the HXRV. A similar increment was derived from this set of test data to account for the sting mount interference; this was accomplished by taking the difference of the blade mount + dummy sting and the blade mount alone data. The primary influence of the sting is an increase in pressure on the nozzle ramp on the lower surface, leading to a small nose-down pitching moment increment. These increments were applied to the sting mount HXRV data in the aero database.

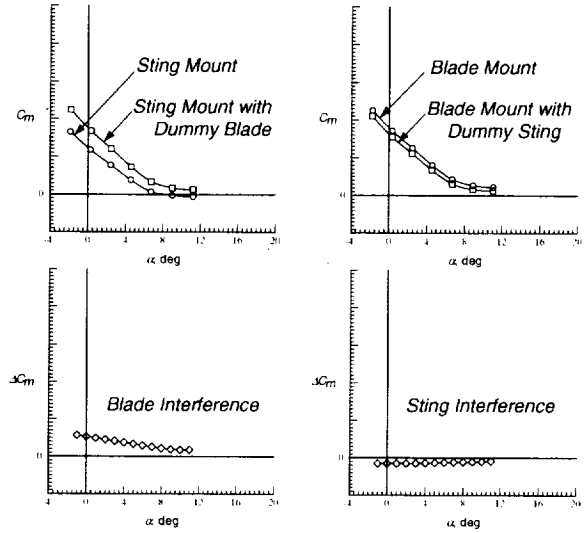

Figure 6. Effects of the sting and blade mount interference on the HXRV Mach 6 basic longitudinal characteristics

The basic cowl-closed airframe lateral-directional characteristics from wind tunnel tests in the LaRC 20-inch Mach 6 Tunnel (Fig. 7) indicate a directionally stable vehicle (positive values of $C_{n\beta}$) over the anticipated flight angle-of-attack range. The configuration also has positive roll stability or effective dihedral (negative values of $C_{l\beta}$) and a nearly constant induced side force at sideslip conditions ($C_{Y\beta}$). Ref. 7 indicates that at Mach 7 flight conditions, approximately 7 degrees of elevon deflection is required to trim the vehicle at 2 degrees angle of attack in the inlet closed configuration, while the inlet-open powered configuration trims at approximately the zero degree elevator position. This design feature is advantageous from a vehicle performance point of view in that inlet-open power-on operation can occur with minimal trim drag penalty. This change in trim elevator setting has an additional indirect effect of increasing the airframe's lateral-directional stability. At the nominal 2 degree angle-of-attack condition, there is a near 60%

increase in the magnitude of the Cl_β term for elevon deflections of 7.5 degrees vs. 0 degrees, and a 17% increase in the $C_{n\beta}$ characteristic. Sideslip induced side force ($C_{Y\beta}$) remains moderately unaffected by elevon position.

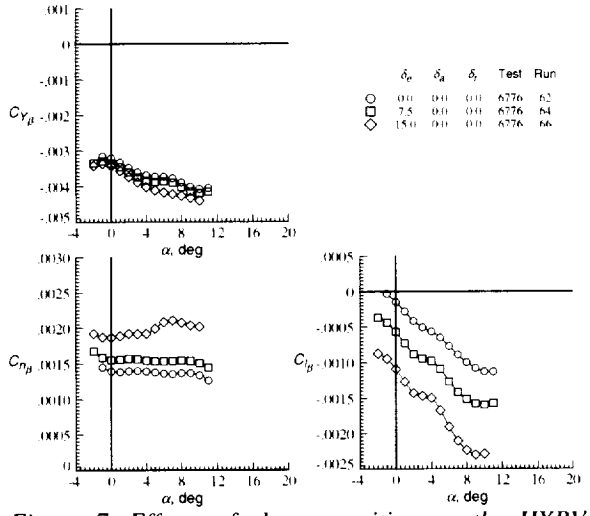

Figure 7. Effects of elevon position on the HXRV basic lateral-directional characteristics

The effect of elevator position on the aileron control power was first identified in data from the 20-Inch Mach 6 Tunnel and is shown in Figure 8. The side force, and yaw and roll moment coefficients due to linearized aileron deflections (per degree) are plotted against vehicle angle-of-attack. For the Hyper-X vehicle, aileron deflections are defined by asymmetric tail deflection about a nominal elevon (tail) position. For example, a +5 degree aileron deflection about a 7.5 degree elevon deflection would require a 5 degree left tail deflection and a 10 degree right tail deflection. The figures indicate a strong dependence of aileron effectiveness on the nominal elevon deflection angle. In particular, the aileron roll effectiveness is almost 70% greater about a 7.5 degree elevon deflection as opposed to a 0 degree elevon deflection.

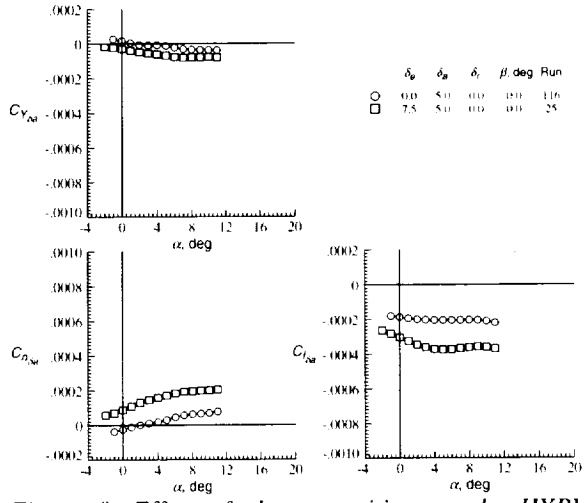

Figure 8. Effect of elevon position on the HXRV aileron control effectiveness

Linearized rudder derivatives, developed using measured force and moment coefficients at 5, 10, 15, and 20 deg rudder deflections relative to 0 deg rudder, are provided for elevator settings of 0 and 7.5 deg in Figures 9 and 10, respectively. Elevator effectiveness is shown to be a function not only of angle of attack, but also of the rudder deflection angle itself, increasing with increasing deflection angle. At low angles-of-attack, the rudders have a moderate amount of effectiveness, which appears to be only minimally affected by the elevon position. However, as angle-of-attack increases, the rudders tend to lose effectiveness in a rather dramatic fashion. In fact, at angles-of-attack approaching 10 degrees, the rudders are almost completely ineffective. This is due primarily to the crossflow separation occurring over the vehicle forebody which tends to bury the vertical tails and rudders in a low energy wake flow (the so-called "hypersonic shielding effect"). The design test point is at an angle-of-attack of two degrees, a condition at which the rudders do provide some degree of directional control authority. However, at a point in the flight trajectory beyond the engine test and post test tares, the vehicle must pull up to an angle-of-attack of approximately 10 degrees in order to generate enough lift to maintain its predetermined altitude profile. At this condition, the rudders will provide little in the way of directional control, and the vehicle will be forced to rely on alternate methods for directional control authority and stability augmentation.

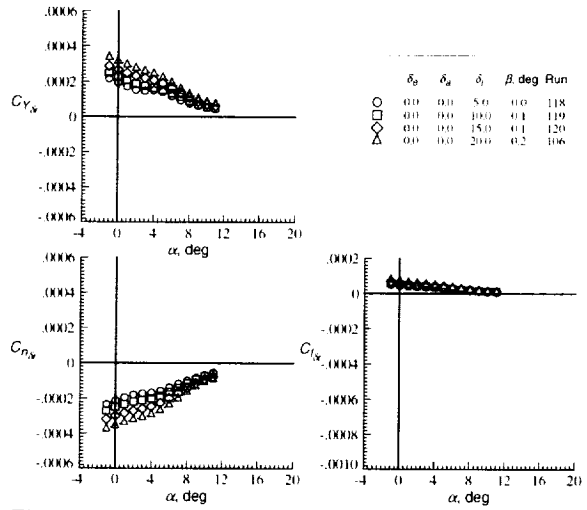

Figure 9. Linearized HXRV rudder control effectiveness at 0 deg elevator position

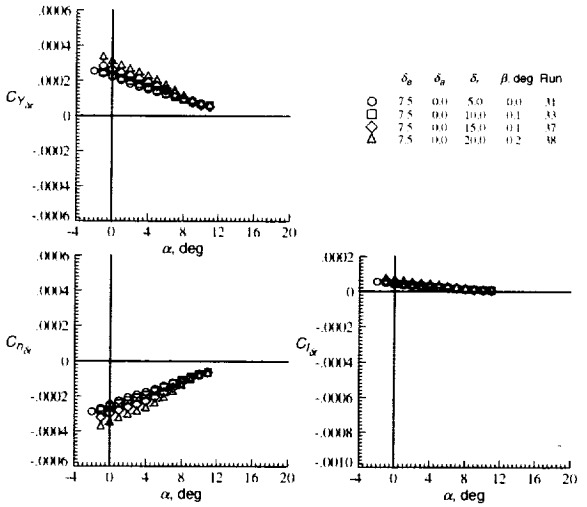

Figure 10. Linearized HXRV rudder control effectiveness at 7.5 deg elevator position

For some vehicles, control power is a function of sideslip. However, for the HXRV, figures 11, 12, and 13 show that the effect of sideslip on the linearized elevator effectiveness, and rudder and aileron effectiveness at both the 0 and 7.5 deg elevator position, respectively, is minimal. As a result, the hypersonic aerodynamic database does not include sideslip sensitivity.

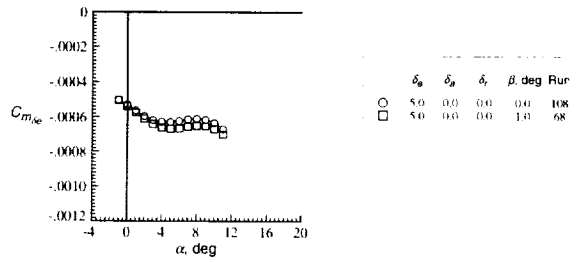

Figure 11. Effect of sideslip on HXRV elevator control effectiveness

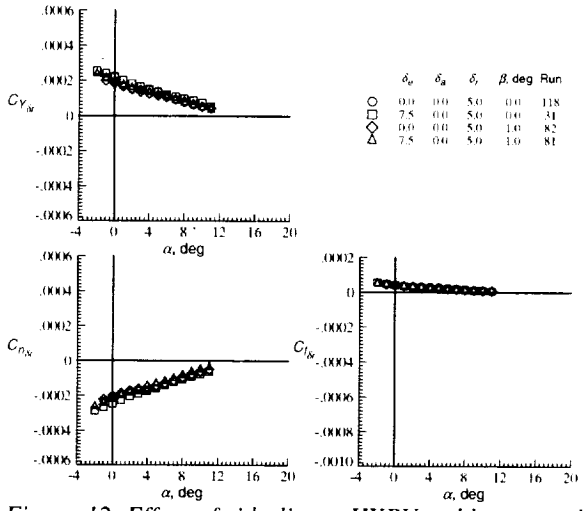

Figure 12. Effect of sideslip on HXRV rudder control effectiveness

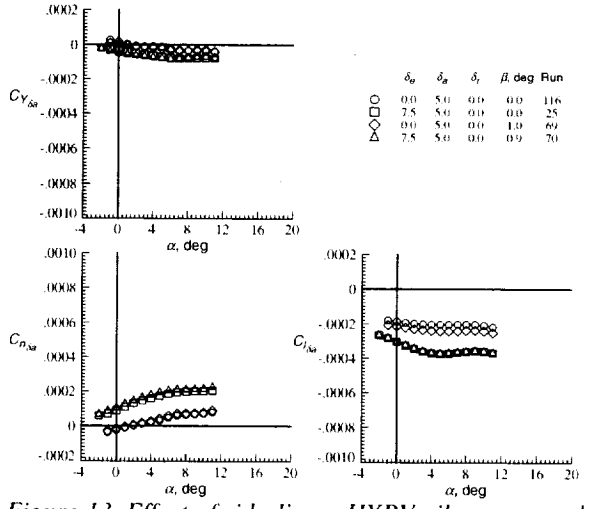

Figure 13. Effect of sideslip on HXRV aileron control effectiveness

Supersonic/Transonic HXRV Aerodynamics

Supersonic and transonic aerodynamic testing was performed using the 20.83% (30-inch) keel line 6 HXRV model shown in Figures 14 and 15. The model was designed to the maximum size permitted based on expected loads and available strain gauge balances for testing in the NASA Langley Unitary Plan Wind Tunnel Test Sections 1 and 2 and the 16-Foot Transonic Tunnel. The model parametrics included full-flying wing deflections (symmetric deflections for elevator, differential deflections for aileron control) in 2.5 deg increments from –20 to +20 deg and rudder deflections (symmetric deflections for rudder control, differential deflections for speed brake) in 5 deg increments from –20 to +20 deg.

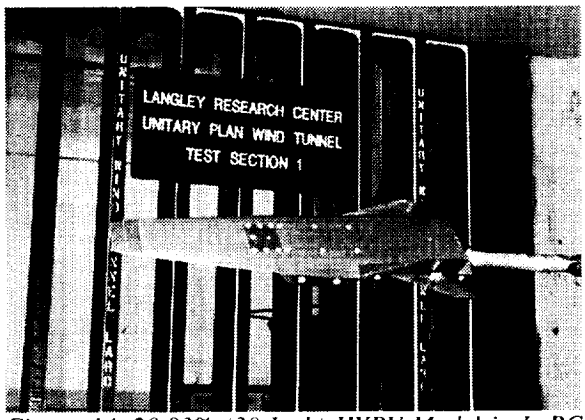

Figure 14. 20.83% (30-Inch) HXRV Model in LaRC Unitary Plan Wind Tunnel

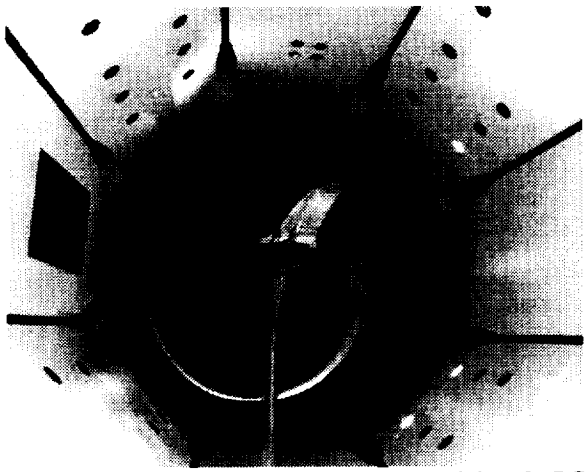

Figure 15. 20.83% (30-Inch) HXRV Model in LaRC 16-Foot Transonic Wind Tunnel

Figures 16, 17, and 18 present the basic longitudinal aerodynamic characteristics for the inlet-closed HXRV at elevator settings representative of trimmed conditions along the trajectory. Figure 16 presents data from Mach 4.6 down to 2.5, Figure 17 from Mach 2.1 down to 1.6, and Figure 18 from Mach 1.2 down to 0.6. Across the supersonic/transonic speed regime, the vehicle demonstrates positive longitudinal stability (negative Cm_α slope) and well-behaved, relatively linear lift characteristics. $C_{m\alpha}$, $C_{L\alpha}$, and C_{Dmin} are shown to be functions of Mach number and reach their extrema at approximately Mach 1.2.

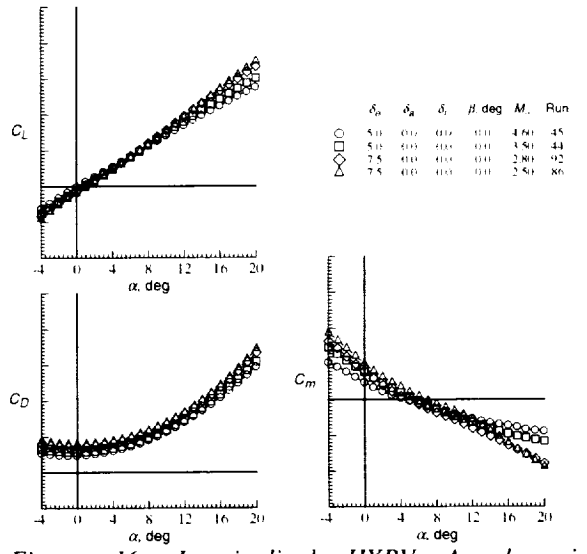

Figure 16. Longitudinal HXRV Aerodynamic Characteristics from Mach 4.6 to 2.5

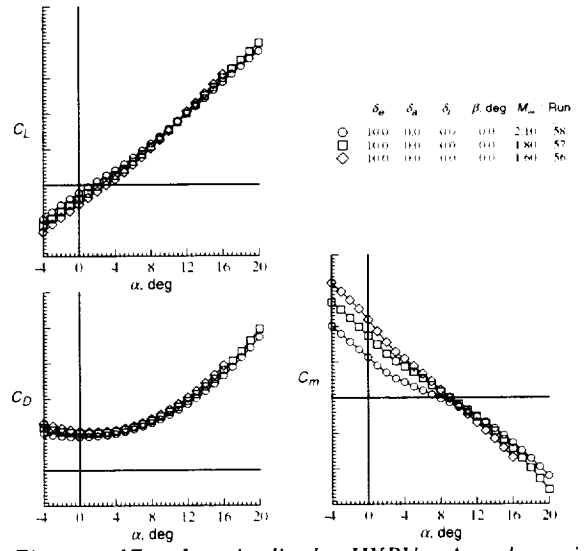

Figure 17. Longitudinal HXRV Aerodynamic Characteristics from Mach 2.1 to 1.6

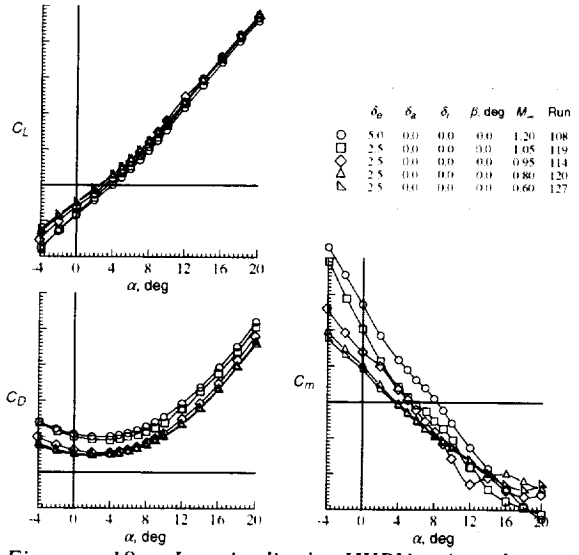

Figure 18. Longitudinal HXRV Aerodynamic Characteristics from Mach 1.2 to 0.6

The cowl-closed lateral-directional characteristics as a function of Mach number are presented in Figure 19. The vehicle is directionally stable (positive values of Cn_β) across the nominal trimmed trajectory. The configuration also has positive roll stability or effective dihedral (negative values of Cl_β), which is diminished with increasing Mach number. Figure 20 presents the aileron effectiveness as a function of Mach number. Aileron effectiveness decreases slightly with Mach number; the figure also illustrates the requirement for control coupling to null the adverse yawing moment with aileron deflection. Rudder effectiveness (Fig. 21) decreases sharply with Mach number. This is due in part to the increased angle of attack in the higher Mach number portion of the trajectory required to generate sufficient lift to maintain its predetermined altitude profile. At higher angles of attack, the rudders are shadowed by the forebody and will provide little directional control.

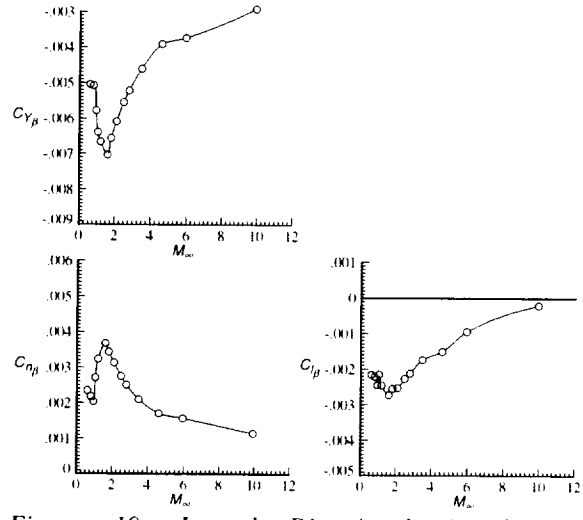

Figure 19. Lateral Directional Aerodynamic Characteristics Along Trimmed Descent Trajectory

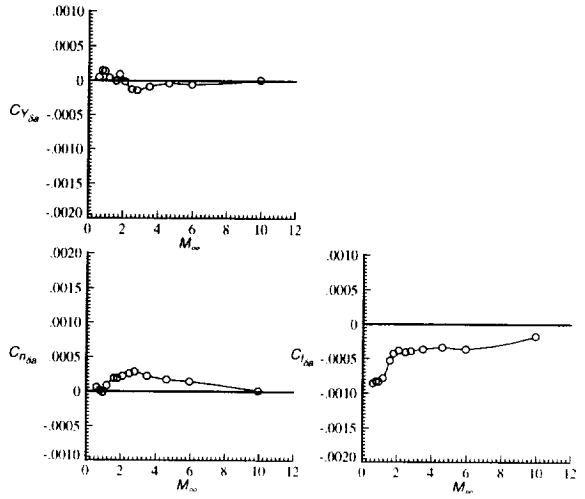

Figure 20. Aileron Effectiveness Along Trimmed Descent Trajectory

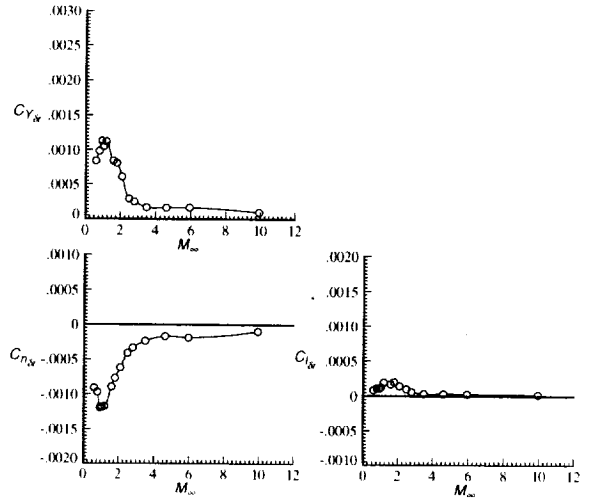

Figure 21. Rudder Effectiveness Along Trimmed Descent Trajectory

Summary

An overview has been provided of the preflight experimental aerodynamics test program for the descent trajectory of the Hyper-X Research Vehicle (HXRV) from engine test to flight termination. Since its inception in 1996, the extensive wind tunnel testing program to evolve and benchmark the current configuration across all phases of the flight trajectory (including transonic to hypersonic launch vehicle boost, stage separation, pre-and post-engine test hypersonic flight, and controlled descent to subsonic flight termination) has utilized 15 models in nine wind tunnels (both government and industry) with a total occupancy of more than 91 weeks. The configuration development is backed by more than 5800 wind tunnel runs. The model design and test philosophy was reviewed. This philosophy focused on use of low-cost, rapid prototyping models with limited parametrics to provide a preliminary configuration screening, followed by optimization with higher fidelity, versatile, multi-use models, followed by precision, specialized models to provide the benchmark control aerodynamics (on- and off-design trajectory) for the flight data book. Additional risk reduction activities included extensive assessment of support interference due to both blade and sting mounting. A brief description of several of the key aerodynamic characteristics of the HXRV from scramjet operation test point to flight termination has been provided. The configuration is statically stable in three axes along the descent trajectory, and has adequate control power provided by the all-moving horizontal tails and the vertical tail-rudder surfaces. The aileron control effectiveness was shown to increase substantially with elevator position at engine test point; this feature has been included in the flight vehicle control law gain scheduling. Both the vehicle's longitudinal stability and the rudder lateral-directional control effectiveness are diminished with increased angle-of-attack beyond about eight degrees. The first flight of the Hyper-X Research Vehicle will be performed at Mach 7 and is currently scheduled for late 2000. The flight trajectory includes multiple parameter identification maneuvers to determine in-flight aerodynamic performance characteristics to provide comparison with and validation of the preflight design and prediction methods for this first-of-its-kind, fully airframe-integrated hydrogen-fueled scramjet powered hypersonic aircraft.

References

1. Tyson, Richard W.: Hyper-X Phase I Program Plan, NASA Langley Research Center Hyper-X Program Office Document HX-419, October 17, 1997

2. Rausch, Vincent L., McClinton, Charles R., and Crawford, J. Larry: HYPER-X: Flight Validation of Hypersonic Airbreathing Technology. XIII ISABE. Chattanooga, TN, September 7-12, 1997, ISABE-97-7024.

3. Bogar, T. J., Alberico, J. F., Johnson, D. B., Espinosa, A. M., and Lockwood, M. K.: Dual-Fuel Lifting Body Configuration Development. AIAA 96-4592, Norfolk VA, Nov. 1996.

4. Hunt, J. L. and Eiswirth, E. A.: NASA's Dual Fuel Airbreathing Hypersonic Vehicle Study. AIAA-CP-96-4591, 7th International Space Planes and Hypersonics Systems and Technology Conference, November 1996.

5. Air Launched Flight Experiment Final Report. McDonnell Douglas Aerospace, June 1995.

6. Eiswirth, E. A.: Dual-Fuel Airbreathing Hypersonic Vehicle Design Study. Interim Report for Phase 3, Hyper-X. Boeing Report 98P0039, June 1998.

7. Engelund , W. C., Holland, S. D., Cockrell, C. E., Jr., and Bittner, R. D.: "Aerodynamic Database Development for the Hyper-X Airframe Integrated Scramjet Propulsion Experiments," AIAA 18th Applied Aerodynamics Conference, August 14-17, 2000, Denver, CO, AIAA-2000-4006

8. Reubush, D. E., Hyper-X Stage Separation – Background and Status. 9th International Space Planes and Hypersonic Systems and Technologies Conference and 3rd Weakly Ionized Gases Workshop, Norfolk, VA, Nov. 1-5, 1999, AIAA-99-4818.

9. Woods, W. C., Holland, S. D.: Hyper-X Stage Separation Wind Tunnel Test Program. AIAA 18th Applied Aerodynamics Conference, August 14-17, 2000, Denver, CO, AIAA-2000-4008.

10. McClinton, C. R., Holland, S. D., Rock, K. E., Engelund, W. C., Voland, R. T., Huebner, L. D., and Rogers, R. C.: Hyper-X Wind Tunnel Program. AIAA 36th Aerospace Sciences Meeting and Exhibit, January 12-15, 1998, Reno, NV, AIAA-98-0553.

11. Allen, V.: Hyper-X Launch Vehicle Aerodynamics Development. AIAA 18th Applied Aerodynamics Conference, August 14-17, 2000, Denver, CO, AIAA-2000-4007.

12. Buning, P. G., Wong, T. C., Dilley, A. D., and Pao, J. L.: Prediction of Hyper-X Stage Separation Aerodynamics Using CFD. AIAA 18th Applied Aerodynamics Conference, August 14-17, 2000, Denver, CO, AIAA-2000-4009.

13. Huebner, L. D., and Tatem, K. E.: CFD Code Calibration and Inlet-Fairing Effects on a 3D Hypersonic Powered-Simulation Model. July 1993, AIAA-93-3041.

14. Cockrell, C. E., Jr., Engelund, W. C., Bittner, R. D., Dilley, A. D., Jentink, T. N., and Frendi, A.: Integrated Aero-Propulsive CFD Methodology for the Hyper-X Flight Experiment. AIAA 18th Applied Aerodynamics Conference, August 14-17, 2000, Denver, CO, AIAA-2000-4010.

15. Huebner, L. D., Rock, K. E., Witte, D. W., Ruf, E. G., and Andrews, E. H., Jr.: Hyper-X Engine Testing in the NASA Langley 8-Foot High Temperature Tunnel. AIAA 36th AIAA/ASME/SAE/ASEE Joint Propulsion Conference, Huntsville, AL, July 2000, AIAA-2000-3605.